Surface Spin Polarization in the Magnetic Response of GeTe Rashba Ferroelectric

A. A. Avakyants, N. N. Orlova[1], A. V. Timonina, N. N. Kolesnikov, E. V. Deviatov

Institute of Solid State Physics of the Russian Academy of Sciences, 142432 Chernogolovka, Russia

We experimentally investigate magnetization reversal curves for a GeTe topological semimetal. In addition to the known lattice diamagnetic response, we observe narrow magnetization loop in low fields, which should not be expected for non-magnetic material. The diamagnetic hysteresis loop is unusual, so the saturation level is negative in positive fields, and the loop is passed clockwise, in contrast to standard ferromagnetic behavior. We show, that the experimental hysteresis curves can not be obtained from standard ferromagnetic ones by adding/subtracting of any linear dependence, or even by considering several interacting magnetic phases. The latter possibility is also eliminated by the remanence plots technique (Henkel or δM plots). We explain our results as a direct consequence of the correlation between ferroelectricity and spin-polarized surface states in GeTe, similarly to magnetoelectric structures.

I. Introduction. Recent renewal of interest to semimetals is mostly connected with topological effects. Topological semimetals are conductors with gapless electronic excitations with band touching in some distinct points, which are protected by topology and symmetry [1]. Similarly to topological insulators [2] and quantum Hall systems [3, 4], topological semimetals have topologically protected surface states. In Weyl semimetals (WSM) every band touching point splits into two Weyl nodes with opposite chiralities due to the time reversal or inversion symmetries breaking. As a result, Fermi arc surface states connect projections of Weyl nodes on the surface Brillouin zone and these surface states inherit the chiral property of the Chern insulator edge states [1].

Usually, spin textures are known in magnetic materials as surface skyrmions [5–13] or spin helix structures [14, 15]. For the magnetic WSMs (broken time reversal symmetry), the Fermi arc surface states were directly visualized in $Co_3Sn_2S_2$ by scanning tunneling spectroscopy [16]. Surface topological textures were visualized in some magnetic semimetals by STM, Lorenz electron microscopy, and magnetic force microscopy [17–19]. Recent investigations show topological protection of skyrmion structures due to their origin from the spin-polarized topological surface states [20].

However, spin textures due to the spin polarization of the Fermi arcs should also take place in non-magnetic WSMs with broken inversion symmetry. Spin- and angle-resolved photoemission spectroscopy technique has demonstrated spin-polarized surface Fermi arcs [21, 22]. Spin-orbit interaction lifts the spin degeneracy of the surface states leading to their in-plane spin polarization, with strongly correlated and predominantly antiparallel spin textures in the neighboring Fermi arcs [23]. As an example of nonmagnetic WSM, spin polarization of the arcs reaches 80 %, as it has been discovered in TaAs [24].

Among nonmagnetic WSM materials, GeTe is of special interest [25–27] due to the reported giant Rashba splitting [27–30]. GeTe is predicted to be topological semimetal in ferroelectric α-phase [31, 32]. Nonlinear Hall effect has been demonstrated in GeTe [33], which is the direct manifestation of finite Berry curvature in topological media [34]. The direct measurement of the Rashba-split surface states of α-GeTe(111) has been experimentally realized thanks to K doping [35]. It has been shown that the surface states are not the result of band bending and that they are decoupled from the bulk states. The giant Rashba splitting of the surface states of α-GeTe is largely arising from the inversion symmetry breaking in the bulk [35].

Surface spin polarization have been directly demonstrated in a magnetic response of topological semimetals with broken time-reversal symmetry [36, 37]. Thus, one can expect a complicated response of a topological semimetal GeTe on the external magnetic field due to the correlation between ferroelectricity and spin tex-

---

[1] e-mail: honna@issp.ac.ru

tures in GeTe [38], similarly to magnetoelectric structures [39].

Here, we experimentally investigate magnetization reversal curves for a GeTe topological semimetal. In addition to the known lattice diamagnetic response, we observe narrow magnetization loop in low fields, which should not be expected for non-magnetic GeTe. We explain our results as a direct consequence of the correlation between ferroelectricity and spin-polarized surface states in GeTe, similarly to magnetoelectric structures.

II. Samples and technique. GeTe single crystals were grown by physical vapor transport in the evacuated silica ampule. The initial GeTe load was synthesized by direct reaction of the high-purity (99.9999 %) elements in vacuum. For the crystals growth, the obtained GeTe serves as a source of vapors: it was melted and kept at 770–780 °C for 24 h. Afterward, the source was cooled down to 350 °C at the 7.5 deg/h rate. GeTe crystals grew during this process on the cold ampule walls above the source.

The GeTe composition is verified by energy-dispersive X-ray spectroscopy. The powder X-ray diffraction analysis confirms single-phase GeTe, see Fig. 1a, the known structure model [28] is also refined with single crystal X-ray diffraction measurements. Ferroelectric polarization and Rashba splitting are defined by the non-centrosymmetric distorted rhombohedral structure (α–GeTe) with space group R3m (# 160) [28]. For our GeTe single crystals, giant Rashba splitting [28] has been confirmed in capacitance measurements [27].
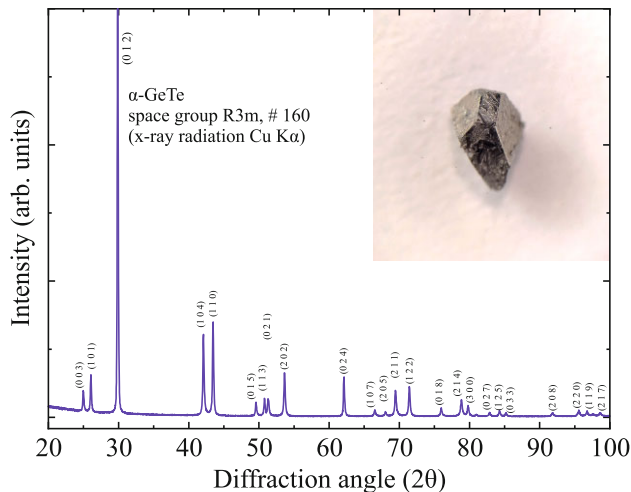

Fig. 1. (Color online) (a) – The X-ray powder diffraction pattern (Cu Kα radiation), which is obtained for the crushed GeTe single crystal. The single-phase α-GeTe is confirmed with the space group R3m (# 160). The inset shows optical image of the crystal

To investigate magnetic properties, we use Lake Shore Cryotronics 8604 VSM magnetometer, equipped with nitrogen flow cryostat. The topological semimetals are essentially three-dimensional objects [1], so we have to select relatively thick (above $0.5\,\mu$m) mechanically exfoliated GeTe flakes. A small (0.82–9.54 mg) flake is mounted to the sample holder by low temperature grease, which has been tested to have a small, strictly linear magnetic response.

We investigate sample magnetization by standard method of the magnetic field gradual sweeping between two opposite field values to obtain magnetization loops. Also, the remanence plots technique (i.e., Henkel or δM plots) is routinely used to evaluate interactions between nanoparticles or grains [40–42].

The technique is based on the comparison of the isothermal remanent magnetization curve (IRM, M_r), and the DC demagnetization remanence curve (DCD, M_d). The IRM curve is obtained on an initially demagnetized sample by applying a positive magnetic field. The DCD curve is measured by first saturating the sample and then measuring the remanence magnetization after application of progressively larger fields of opposite direction. For a system of noninteracting single-domain particles with uniaxial anisotropy, the IRM and DCD are related to each other via the Wohlfarth equation

$$M_d(H) = M_{rs} - 2M_r(H),$$

where M_{rs} is the saturation remanence and H is the applied magnetic field.

The δM or Henkel plot is a direct measure of the deviation from the linearity:

$$\delta M(H) = M_d(H) - [M_{rs} - 2M_r(H)].$$

Interparticle interactions are detected through the appearance of a negative dip (demagnetizing interactions, typically dipolar one) or a positive peak (magnetizing, usually exchange, interactions) in the δM plots, whereas $\delta M = 0$ has generally been taken as an indication of the absence of interactions [41, 43]. In other words, positive and negative δM contributions indicate more than one phase [44].

III. Experimental results. Figure 2 shows magnetization loops at 100 K temperature for the 6.69 mg GeTe flake. The overall $M(H)$ behavior shows the diamagnetic response, which is known for the bulk GeTe mostly due to the lattice defects [45]. From the linear diamagnetic dependence we can estimate the slope as $-3 \cdot 10^{-6}\,$emu/cm^3, this estimation well corresponds to the reported GeTe volume susceptibility [45]. The $M(H)$ curves show some angle dependence, as it is confirmed by the direct $M(\alpha)$ measurement in the inset to

Fig. 2: we observe about 20 % modulation of the $M(\alpha)$ with 180° periodicity in the magnetic field 15 kOe. This shallow angle dependence seems to originate from the shape of the exfoliated flake with well-developed cleaved surface.
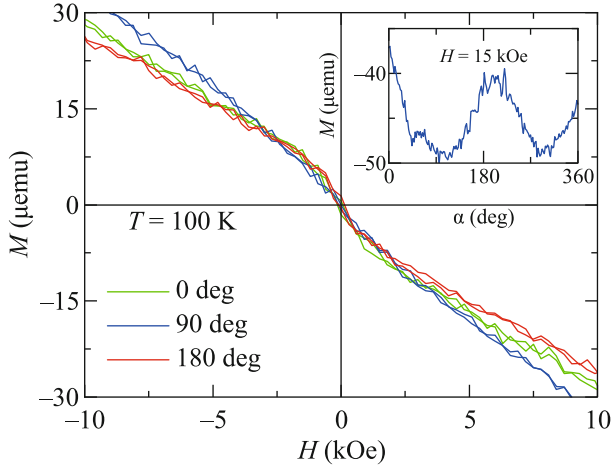

Fig. 2. (Color online) Magnetization curves at 100 K temperature for the 6.69 mg GeTe flake. The overall $M(H)$ behavior shows diamagnetic response [45], which is accompanied by the clearly visible kink in $M(H)$ dependence at low fields, within ±1 kOe interval. The $M(H)$ curves are shown for several angles α between the sample holder and magnetic field. Inset shows $M(\alpha)$ dependence: we observe about 20 % modulation of the $M(\alpha)$ with 180° periodicity in the magnetic field 15 kOe. This shallow angle dependence seems to originate from the shape of the exfoliated flake with well-developed cleaved surface

The most striking experimental result is the clearly visible kink in $M(H)$ dependence at low fields, within ±1 kOe interval, see Fig. 2. The kink can be seen for any sample orientation. Diamagnetic response with low-field kink can be qualitatively reproduced for different GeTe flakes. For example, Fig. 3a shows $M(H)$ curves for 9.54 and 0.82 mg samples, respectively. We should conclude, that the standard linear diamagnetic response is accompanied by narrow magnetization loop, which should not be the case for the diamagnetic GeTe.

First of all, we should exclude possible systematic errors. In our experiment, the GeTe sample is mounted to the sample holder by low-temperature grease, which has some diamagnetic response at 100 K. We show in Fig. 3b by black dashed curves, that without GeTe sample we obtain strictly linear diamagnetic dependence (the amount of grease is increased to have similar level of the signal as for the 9.54 mg GeTe sample, the red curve). The linear curve is obtained from the same setup, the same sample holder, the same grease, and at

the same temperature. Thus, our unusual diamagnetic response with low-field kink is from the GeTe sample, not from the setup.

The diamagnetic slope crudely scales with the sample mass, as it should be expected for the lattice-defects-induced response: it is increased by approximately a factor of two for the 1.5 mass increase, compare Figs. 2 and 3a, the red curve; also, the slopes differ by 8 times for two flakes in Fig. 3, which is near the sample mass ratio 11.6. The ≈ 25 % discrepancy can to be ascribed to the different shape of the exfoliated flakes, due to the arbitrary orientation of the cleaved surfaces (cp. with the 20 % modulation of the $M(\alpha)$ in the inset to Fig. 2).

The low-field kink is better seen for the smaller samples, so even low-field hysteresis can be seen for the smallest 0.82 mg GeTe flake in Fig. 3a. The hysteresis is shown in detail in Fig. 4 for all three samples. We use curve averaging (8 curves) to increase the signal/noise ratio. The linear diamagnetic slope is subtracted from the averaged curves to highlight the nonlinear low-field behavior.

First of all, all three samples show clear low-field hysteresis in Fig. 4. To our surprise, the saturation level is negative in positive fields, and the loop is passed clockwise, in contrast to usual ferromagnetic hysteresis.

We wish to note, that our unusual diamagnetic loop can not be considered as inverted hysteresis in the common sense (e.g. in terms of [46] and references therein). Indeed, usual inverted hysteresis implies two magnetic phases: the inversion reflects the phase interaction in this case, so one magnetic phase provides a bias field to the second one [47]. This bias field forces the magnetization reversal even before the reversal of the external field, so the loop is passed clockwise [36].

In our case, we observe unusual diamagnetic loop, where the saturation level is inverted instead of the switching field. The saturation level is negative in positive fields, it is reversed after the external field reversal.

Also, the experimental curves in Fig. 4 can not be continuously transformed to the standard ferromagnetic one (the saturation level is positive in positive fields) by adding/subtracting of any linear dependence. Standard ferromagnetic loop, as been added to the linear diamagnetic curve, can not invert the saturation levels around the zero field, as it is shown in Fig. 3c. This model loop is therefore passed counterclockwise, in contrast to the experimental curves in Fig. 4. The qualitative difference between the model and experimental curves excludes any possible contribution from any magnetic contamination, e.g. magnetic impurities [48].

The saturation level value depends on the sample mass in Fig. 4a and c, but without strict proportional-
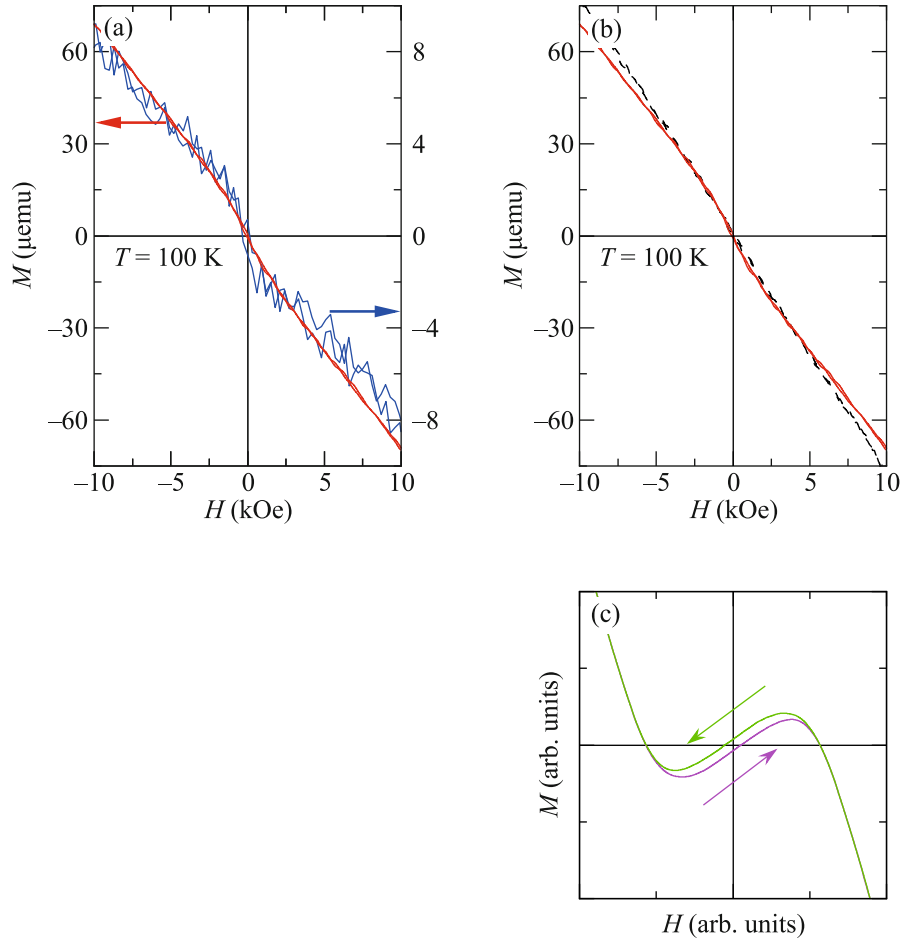
Fig. 3. (Color online) (a) – Magnetization loops at 100 K temperature for two 9.54 and 0.82 mg GeTe flakes, see the left and the right axes, respectively. The diamagnetic slope crudely scales with the sample mass. The linear curves with low-field kink are qualitatively similar to the behavior in Fig. 2. The low-field kink is better seen for the smaller sample, so even low-field hysteresis can be seen for the smallest 0.82 mg GeTe flake. (b) – Strictly linear diamagnetic curve (black dashed line) is shown for our setup without a GeTe flake in comparison with the 9.54 mg Gete sample nonlinear response (red). In our experiment, the GeTe sample is mounted to the sample holder by low-temperature grease, which has small diamagnetic response at 100 K. For the black reference curve, the amount of grease is increased to have similar level of the signal as for the red one. In contrast to the GeTe response (red curve), sample holder and grease are characterized strictly linear diamagnetic dependence (black). (c) – A model curve, where a standard ferromagnetic loop is added to the linear diamagnetic dependence. This procedure can not invert the saturation levels near the zero field, and the model loop is passed counterclockwise, in contrast to the experimental curves in Fig. 4. The qualitative difference between the model and experimental curves excludes any possible contribution from any magnetic contamination, e.g. magnetic impurities [48]

ity: it is increased from $3\,\mu$emu in (a), for the 6.69 mg GeTe flake, to $4.5\,\mu$emu in (c), for the 9.54 mg one. However, it is below $1\,\mu$emu in (b), for the smallest, 0.82 mg GeTe flake, but the signal is noisy here. The hysteresis width at zero M level (coercitivity) is different for all three samples, but no reasonable dependence can be seen in Fig. 4a–c. The hysteresis is not sensitive to temperature below 200 K, as it is shown in Fig. 4a and c. After subtracting the diamagnetic slope, the low-field hysteresis is not sensitive to the field orientation within our accuracy, see Fig. 4d.

As it is mentioned above, the hysteresis in Fig. 4 can not be connected with usual ferromagnetic phases. This can be also verified by the remanence plots technique (i.e., Henkel or δM plots). Figure 5 shows both the initial $M_r(H)$, $M_d(H)$ curves and the calculated $\delta M(H)$. $\delta M(H)$ for GeTe varies around zero with significant amplitude, in contrast to the reference δM curve, obtained for the standard nickel sample. In the latter case, well-defined negative δM dip corresponds to the dipolar interaction between ferromagnetic domains [41, 43, 44]. Thus, the remanence plot in Fig. 5 is also inconsistent
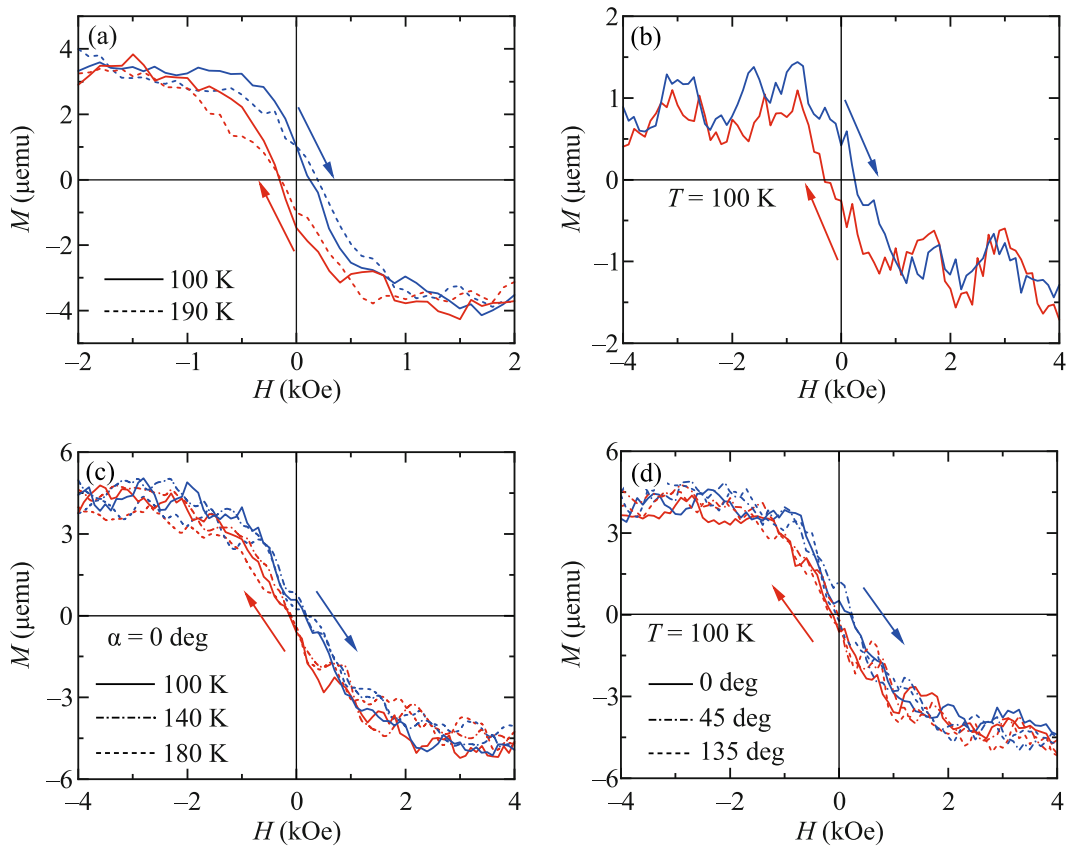
Fig. 4. (Color online) The low-field hysteresis region for all three samples. For every field sweep direction, we use curve averaging (8 curves) to increase the signal/noise ratio. The diamagnetic slope is subtracted from the averaged curves to highlight the nonlinear low-field behavior. (a) – Curves for the 6.69 mg GeTe flake at two temperatures, 100 K (solid) and 190 K (dash). (b) – $M(H)$ curves for the smallest, 0.82 mg GeTe flake, at 100 K. (c), (d) – Hysteresis for the 9.54 mg flake at different temperatures (c) and sample orientation (d). For every sample, the saturation level is negative in positive fields, and the loop is passed clockwise, in contrast to usual ferromagnetic hysteresis

with usual ferromagnetic behavior, i.e. with the magnetic contamination of the sample.

IV. Discussion. As a result, we observe that the lattice diamagnetic response is accompanied by the low-field hysteresis loop in GeTe. In contrast to usual ferromagnetic hysteresis, the saturation level is negative in positive fields so the loop is passed clockwise.

As it is discussed above, the observed unusual diamagnetic loop can not be considered as known inverted hysteresis [36, 46, 47], which originates from several interacting magnetic phases, since the bias field can not invert the saturation levels. Also, the remanence plots technique (i.e., Henkel or δM plots) does not confirm several magnetic phases for our GeTe flakes.

GeTe composition is verified by energy-dispersive X-ray spectroscopy and the powder X-ray diffraction analysis. The obtained volume susceptibility $-3 \cdot 10^{-6}$ well corresponds to the known values [45]. Thus, there is no magnetic impurities in our GeTe crystals. Also, different

types of magnetic contamination can only add a standard ferromagnetic loop to the sample response [37, 48], which is excluded in Fig. 3, see the corresponding text. Thus, any type of magnetic impurities can not be responsible for the observed unusual diamagnetic loop.

To rule out systematic error of the VSM, like possible remanent field in the electric magnet, etc., we demonstrate strictly linear diamagnetic dependence without GeTe sample for the same setup, the same sample holder, the same grease, and at the same temperature in Fig. 3b.

For these reasons, we should consider possible contribution from the surface-state induced spin textures [35] in α-GeTe(111). Spin-polarized surface states can, in principle, give significant contribution into the overall magnetic response [36] due to the fact, that in topological semimetals one have nearly complete spin polarization of the surface states. For example, spin polarization of the arcs can be as high as 80 % in nonmag-
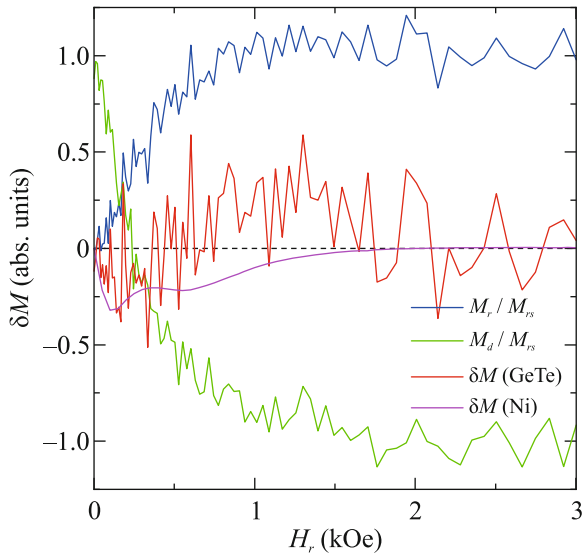
Fig. 5. (Color online) Henkel or remanence δM plot for 6.69 mg GeTe flake at 100 K temperature. The initial $M_r(H), M_d(H)$ curves (blue and green ones, respectively), give the $\delta M(H)$ (red) curve. Within the accuracy of experiment, $\delta M(H)$ behavior can not definitely confirm several magnetic phases for our GeTe flakes. For comparison, a reference fully negative δM curve (magenta) is shown, as obtained for the standard nickel sample. Thus, the remanence plot is also inconsistent with usual ferromagnetic behavior, e.g. known for the magnetic impurities

netic TaAs [24]. However, the direct response of surface states leads to usual ferromagnetic loop, which might be inverted in the sense of usual inverted hysteresis [36].

On the other hand, direct correlation between ferroelectricity and spin textures was demonstrated in GeTe [38]. Both the giant Rashba splitting of the surface states and bulk ferroelectricity are largely arising from the inversion symmetry breaking [35]. For our GeTe single crystals, giant Rashba splitting [28] and bulk ferroelectricity have been confirmed in capacitance measurements [27]. Even for the conductive materials [49–52], ferroelectric polarization can be affected or switched by external field in $MoTe_2$ and WTe_2 topological semimetals [53, 54], and also in SnSe and SnTe semiconductors [55, 56]. Ferroelectric polarization can be controlled by the in-plane current-induced electric field in WTe_2 and SnSe thin films [57, 58].

Thus, GeTe single crystal can be considered as magnetoelectric heterostructure [59, 60], which can be responsible for the observed unusual diamagnetic loop. In magnetoelectrics, due to the coupling among the different degrees of freedom (ferroelectricity, ferromagnetism, or ferroelasticity) leading to these ordered states, the order parameter of one state can be controlled by tuning parameters different from their conjugate variable [61]. In particular, this coupling leads to the magnetization oscillations [62] and the oscillatory Hall effect [39].

In the conditions of our experiment, variation of the magnetic field leads to appearance of the electric field due to the magnetoelectric coupling [39, 63]. Electric field affects spin textures in GeTe [38], which, subsequently, affects magnetization response [59–61, 64]. In this case, the unusual diamagnetic loop appears due to the delay of the magnetic response to the external field, since electric fields are coupled to strain in ferroelectrics [65]. This effect can be clearly seen mostly around zero field, while the experimental curves are not strictly linear also in high fields, compare red and black curves in Fig. 3b. Thus, the unusual diamagnetic loop is a direct consequence of correlation between ferroelectricity and spin-polarized surface states in GeTe.

V. Conclusion. As a conclusion, we experimentally investigate magnetization reversal curves for a GeTe topological semimetal. In addition to the known lattice diamagnetic response, we observe narrow magnetization loop in low fields, which should not be expected for non-magnetic GeTe. The diamagnetic hysteresis loop is unusual, so the saturation level is negative in positive fields, and the loop is passed clockwise, in contrast to standard ferromagnetic behavior. The experimental hysteresis curves can not be obtained from standard ferromagnetic ones by adding/subtracting of any linear dependence, or even by considering several interacting magnetic phases, which is also eliminated by the remanence plots technique (Henkel or δM plots). We explain our results as a direct consequence of the correlation between ferroelectricity and spin-polarized surface states in GeTe, similarly to magnetoelectric structures.

Conflict of interest. The authors of this work declare that they have no conflicts of interest.

1. N. P. Armitage, E. J. Mele, and A. Vishwanath, Rev. Mod. Phys. **90**, 015001 (2018); arxiv:1705.01111.

2. M. Z. Hasan and C. L. Kane, Rev. Mod. Phys. **82**, 3045 (2010).

3. M. Büttiker, Phys. Rev. B **38**, 9375 (1988).

4. E. V. Deviatov, Phys.-Uspekhi **50**(2), 197 (2007).

5. S.-X. Wang, H.-R. Chang, and J. Zhou, Phys. Rev. B **96**, 115204 (2017).

6. H.-R. Chang, J. Zhou, S.-X. Wang, W.-Y. Shan, and D. Xiao, Phys. Rev. B **92**, 241103 (2015).

7. M. M. Valizadeh, Int. J. Mod. Phys. B **30**, 1650234 (2016).

8. J.-J. Zhu, D.-X. Yao, S.-C. Zhang, and K. Chang, Phys. Rev. Lett. **106**, 097201 (2011).

9. K. Everschor-Sitte, J. Masell, R. M. Reeve, and M. Klaui, J. Appl. Phys. **124**, 240901 (2018).

10. Y. Y. Dai, H. Wang, P. Tao, T. Yang, W. J. Ren, and Z. D. Zhang, Phys. Rev. B **88**, 054403 (2013).

11. C. Back et al., Journal of Physics D: Applied Physics **53**, 363001 (2020).

12. J. Kang and J. Zang, Phys. Rev. B **91**, 134401 (2015).

13. S. Muhlbauer, B. Binz, F. Jonietz, C. Pfleiderer, A. Rosch, A. Neubauer, R. Georgii, and P. Boni, Science **323**, 915тАУ919 (2009).

14. B. A. Bernevig, J. Orenstein, and S.-C. Zhang, Phys. Rev. Lett. **97**, 236601 (2006).

15. J. D. Koralek, C. P. Weber, J. Orenstein, B. A. Bernevig, Sh.-Ch. Zhang, S. Mack, and D. D. Awschalom, Nature **458**, 610тАУ613 (2009).

16. N. Morali, R. Batabyal, P. K. Nag, E. Liu, Q. Xu, Y. Sun, B. Yan, C. Felser, N. Avraham, and H. Beidenkopf, Science **365**, 1286 (2019); DOI: 10.1126/science.aav2334.

17. M.-G. Han, J. A. Garlow, Y. Liu, H. Zhang, J. Li, D. DiMarzio, M. W. Knight, C. Petrovic, D. Jariwala, and Y. Zhu, Nano Lett. **19**(11), 7859 (2019).

18. B. Ding, Z. Li, G. Xu, H. Li, Zh. Hou, E. Liu, X. Xi, F. Xu, Y. Yao, and W. Wang, Nano Lett. **20**, 868 (2020).

19. G. D. Nguyen, J. Lee, T. Berlijn, Q. Zou, S. M. Hus, J. Park, Zh. Gai, Ch. Lee, and A.-P. Li, Phys. Rev. B **97**, 014425 (2018).

20. Y. Araki, Ann. Phys. (Berlin) **532**, 1900287 (2020).

21. P. K. Das, D. D. Sante, I. Vobornik et al. (Collaboration), Nat. Commun. **7**, 10847 (2016).

22. B. Feng, Y.-H. Chan, Y. Feng et al. (Collaboration), Phys. Rev. B **94**, 195134 (2016).

23. D. A. Pshenay-Severin, Y. V. Ivanov, A. A. Burkov, and A. T. Burkov, J. Phys. Condens. Matter **30**, 135501 (2018).

24. S.-Y. Xu, I. Belopolski, D. S. Sanchez et al. (Collaboration), Phys. Rev. Lett. **116**, 096801 (2016).

25. S. Varotto, L. Nessi, S. Cecchi et al. (Collaboration), Nat. Electron. **4**, 740 (2021).

26. S. Picozzi, Frontiers in Physics Condensed Matter Physics **2**, 10 (2014).

27. N. N. Orlova, A. V. Timonina, N. N. Kolesnikov, and E. V. Deviatov, Physica B: Condensed Matter **647**, 414358 (2022); https://doi.org/10.1016/j.physb.2022.414358.

28. D. Di Sante, P. Barone, R. Bertacco, and S. Picozzi, Adv. Mater. **25**, 509 (2013).

29. M. Liebmann, Ch. Rinaldi, D. Di Sante et al. (Collaboration), Adv. Mater. **28**, 560 (2016).

30. J. Krempaský, H. Volfová, S. Muff et al. (Collaboration), Phys. Rev. B **94**, 205111 (2016).

31. A. Lau and C. Ortix, Phys. Rev. Lett. **122**, 186801 (2019).

32. J. Krempaský, L. Nicolaï, M. Gmitra, H. Chen, M. Fanciulli, E. B. Guedes, M. Caputo, M. Radović, V. V. Volobuev, O. Caha, G. Springholz, J. Minár, and J. H. Dil, Phys. Rev. Lett. **126**, 206403 (2021).

33. N. N. Orlova, A. V. Timonina, N. N. Kolesnikov, and E. V. Deviatov, Chin. Phys. Lett. **40**, 077302 (2023); https://doi.org/10.1088/0256-307X/40/7/077302.

34. I. Sodemann and L. Fu, Phys. Rev. Lett. **115**, 216806 (2015).

35. G. Kremer, T. Jaouen, B. Salzmann, L. Nicolaï, M. Rumo, C. W. Nicholson, B. Hildebrand, J. H. Dil, J. Minár, G. Springholz, J. Krempaský, and C. Monney, Phys. Rev. Research **2**, 033115 (2020).

36. A. A. Avakyants, N. N. Orlova, A. V. Timonina, N. N. Kolesnikov, and E. V. Deviatov, J. Magn. Magn. Mater. **573**, 170668 (2023); https://doi.org/10.1016/j.jmmm.2023.170668.

37. N. N. Orlova, A. A. Avakyants, A. V. Timonina, N. N. Kolesnikov, and E. V. Deviatov, Phys. Rev. B **107**, 155137 (2023); https://doi.org/10.1103/PhysRevB.107.155137.

38. Ch. Rinaldi, S. Varotto, M. Asa, J. Sławinska, J. Fujii, G Vinai, S. Cecchi, D. Di Sante, R. Calarco, I. Vobornik, G. Panaccione, S. Picozzi and R. Bertacco, Nano Lett. **18**, 2751 (2018).

39. P. C. Lou, R. G. Bhardwaj, A. Katailiha, W. P. Beyermann, and S. Kumar, Phys. Rev. B **109**, L081113 (2024); https://doi.org/10.1103/PhysRevB.109.L081113.

40. J. M. D. Coey, *Magnetism and Magnetic Materials*, Cambridge University Press, Cambridge (2009).

41. P. E. Kelly, K. O'Grady, P. I. Mayo, and R. W. Chantrell, IEEE Trans. Magn. **25**, 3881 (1989).

42. O. Henkel, Phys. Status Solidi B **7**, 919 (1964).

43. P. Bender, F. Krämer, A. Tschöpe, and R. Birringer, J. Phys. D: Appl. Phys. **48**, 145003 (2015).

44. J. Sánchez, C. Sánchez, and A. G. Santana, J. Magn. Magn. Mater. **294**, 226 (2005).

45. J. E. Lewis, Phys. Status Solidi **38**, 131 (1970).

46. I. Soldatov, P. Andrei, and R. Schaefer, IEEE Magn. Lett. **11**, 2405805 (2020).

47. M. Saghayezhian, Zh. Wang, H. Guo, R. Jin, Y. Zhu, J. Zhang, and E. W. Plummer, Phys. Rev. Research **1**, 033160 (2019).

48. F. W. Constant and J. M. Forwalt, Phys. Rev. **56**, 373 (1939).

49. Y.-W. Fang and H. Chen, Commun. Mater. **1**, 1 (2020).

50. A. Filippetti, V. Fiorentini, F. Ricci, P. Delugas, and J. Iniguez, Nat. Commun. **7**, 11211 (2016).

51. T. H. Kim, D. Puggioni, Y. Yuan, L. Xie, H. Zhou, N. Campbell, P. J. Ryan, Y. Choi, J.-W. Kim, J. R. Patzner, S. Ryu, J. P. Podkaminer, J. Irwin, Y. Ma, C. J. Fennie, M. S. Rzchowski, X. Q. Pan, V. Gopalan, J. M. Rondinelli, and C. B. Eom, Nature **533**, 68 (2016).

52. Z. Fei, W. Zhao, T. A. Palomaki, B. Sun, M. K. Miller, Z. Zhao, J. Yan, X. Xu, and D. H. Cobden, Nature **560**, 336 (2018).

53. Sh. Yuan, X. Luo, H. L. Chan, Ch. Xiao, Y. Dai, M. Xie, and J. Hao, Nature Commun. **10**, 1775 (2019).

54. P. Sharma, F.-X. Xiang, D.-F. Shao, D. Zhang, E. Y. Tsymbal, A. R. Hamilton, and J. Seide, Sci. Adv. **5**(7), eaax5080 (2019).

55. K. Chang, F. Küster, B. J. Miller, J.-R. Ji, J.-L. Zhang, P. Sessi, S. Barraza-Lopez, and S. S. P. Parkin, Nano Lett. **20**(9), 6590 (2020).

56. K. Yasuda, X. Wang, K. Watanabe, T. Taniguchi, and P. Jarillo-Herrero, Science **372**, 6549 1458 (2021).

57. N. N. Orlova, N. S. Ryshkov, A. V. Timonina, N. N. Kolesnikov, and E. V. Deviatov, JETP Lett. **113**, 389 (2021).

58. N. N. Orlova, A. V. Timonina, N. N. Kolesnikov, and E. V. Deviatov, Phys. Rev. B **104**, 045304 (2021).

59. C. Israel, S. Kar-Narayan, and N. D. Mathur, Appl. Phys. Lett. **93**, 173501 (2008).

60. Zh. Shen, Sh. Dong, and X. Yao, arxiv:2310.04810 (2023).

61. A. O. Fumega and J. L. Lado, 2D Materials **9**, 025010 (2022); https://doi.org/10.1088/2053-1583/ac4e9d

62. N. N. Orlova, A. A. Avakyants, A. V. Timonina, N. N. Kolesnikov, and E. V. Deviatov; arXiv:2309.08392.

63. W. Xun, Ch. Wu, H. Sun, W. Zhang, Y.-Zh. Wu, and P. Li, arXiv:2403.01070.

64. V. Gunawan and N. A. K. Umiati, International Journal of Electrical and Computer Engineering (IJECE) **8**, 4823 (2018); DOI: 10.11591/ijece.v8i6.pp4823-4828.

65. W. Hou, A. Azizimanesh, A. Sewaket, T. Pena, C. Watson, M. Liu, H. Askari, and S. M. Wu, Nat. Nanotechnol. **14**, 668 (2019).